Journal Name

ARTICLE TYPE

Cite this: DOI: 00.0000/xxxxxxxxxx

A gradient-descent adjoint method for the reconstruction of boundary conditions in a river flow nitrification model

Geovanny Gordillo,*[a] Mario Morales-Hernández,[b] and Pilar García-Navarro[a]

Received Date
Accepted Date

DOI: 00.0000/xxxxxxxxxx

One of the reasons of the limited applicability of predictive water quality models is the lack of data from monitoring control stations that are required as input. In this context, the main novelty of the present work is the recovery of information on the state variables present in a water quality model through measured data at a target downstream location. The reconstruction of the upstream boundary condition is the goal of the present work. For this purpose, an adjoint-state method is developed to find the sensitivities of the functional with respect to variations on the upstream boundary conditions of the model. The resolution of both forward and backward problems ensures strong, accurate and reliable solutions in both steady state and unsteady scenarios. The different cases demonstrate that the method is able to reconstruct any observed distribution with little computational effort, including the heat balance with all its external inputs.

1 Introduction

Predictive models can be useful to represent physical processes that occur in nature such as overland water flow, solute transport or sediment transport among others, using physically based partial differential equations [1]. For the numerical resolution of these models, the initial conditions must be stated and boundary conditions at the limits of the computational domain are needed in addition to a robust numerical scheme. The first data set is established within the whole domain, at the start of the simulation. The availability of this information is crucial for the reliability of the simulation models, so that their predictions are accurate when compared with measured data at specific control sections. However this information is not always available with the necessary frequency and quality. Therefore, it is essential to have a mechanism to reconstruct initial conditions and/or boundary conditions that minimize the differences between predicted and observed data. The present work is focused on the reconstruction of the upstream water quality boundary condition in the context of physically based 1D models provided that the hydrodynamic upstream and downstream boundary conditions as well as all initial conditions are known.

The indirect inverse method emerges as a robust and theoretically solid technique to minimize the differences between model results and observed data [2]. There are two large groups of methods to solve this type of inverse problems: the gradient descent methods and the population search methods. Numerous studies have been carried out for both. As an example of the second type, Zou *et al.* [3] propose a genetic algorithm integrated into a neural network to solve problems of inverse water quality modeling. Azad *et al.* [4] investigated adaptive neuro fuzzy inference system with particle swarm optimization (ANFIS-PSO) and ant colony optimization for continuous domains ($\mathrm{ANFIS}-\mathrm{ACO_R}$) to estimate water quality parameters. Among the gradient descent type, other studies have been developed in order to minimize the environmental impact produced by the discharge of one or multiple point sources of conservative solutes [5]. The gradient technique has also been proposed to determine the sensitivity of a solute concentration to real-time changes in load intensity at a remote source. In this context, the adjoint equation of the fate and transport was used to evaluate this sensitivity [6,7]. This formulation was also used to calculate the sensitivity of dissolved oxygen (DO) in a stream over carbonaceous biological oxygen demand (CBOD) discharges [8]. In the same line, more ambitious works have been elaborated to calculate the sensitivity of the DO with respect to the load vector and the reaction coefficients that make up the eutrophication cycle [9,10]. The application of the adjoint method has also been extended to water distribution systems to observe the effect produced by the variation of some parameters such as the location of the source and the reaction rate of the pollutant at the system output [11].

[a] *Fluid Mechanics, University of Zaragoza/ LIFTEC-CSIC, C/María de Luna, Edif. Torres Quevedo, 50018, Zaragoza, Spain; E-mail: ggordillo@unizar.es*
[b] *Computational Science and Engineering Division; Oak Ridge National Laboratory Oak Ridge, TN (USA), 37831.*

The theory of the adjoint problem has also been applied to identify the Manning roughness coefficient in a channel network in one dimension (1D) using a Quasi-Newton Limited-Memory algorithm[12]. In this hydraulic context, the analysis of the sensitivity of shallow-water flow to boundary changes in depth and discharge was also developed to control water waves in fluvial systems and estuaries, allowing a practical use in the applications of shallow water equations[13,14]. A more ambitious implementation of this technique was reported[15] that used the continuous adjoint approximation to reconstruct the boundary conditions in a 2D model using the Graphics Processing Unit (GPU) solved both the physical system and the adjoint, achieving notable reduction in the computational burden.

In the matter of water quality in rivers, the adjoint problem has focused more on the analysis of the sensitivity at a point source and model parameters[7], missing a study of the sensitivities of the functional to the upstream boundary condition. Therefore, in this framework, the main novelty of this work is to determine the sensitivity of a function error with respect to the upstream or inlet boundary conditions present in a nitrification model, including the influence of temperature. Through this process, it is possible to recover upstream boundary conditions of the different chemical species involved in the water quality model from downstream measured data and knowing the hydrodynamic information in both steady state and unsteady scenarios.

The resolution of both physical and adjoint problem is carried out using an explicit finite volume scheme based on Roe's linearization. The control of the sensitivity produced by the adjoint resolution is determined by the gradient descent method. Both quality and hydrodynamic processes are resolved in 1D.

The present work is organized as follows: in Section 2 the mathematical development of the adjoint equations for different levels of complexity is presented. Section 3 is devoted to the numerical resolution of both the physical and adjoint system. The evaluation of the numerical method with synthetic and real cases is presented in Section 5. Finally, conclusions are included in Section 6.

2 Mathematical adjoint models for the simulation of the scalar transport

The expressions that allow to solve the hydrodynamic variables (the flow rate Q [L^3T^{-1}] and the cross section area A [L^2]) are the shallow water equations. This system of equations is expressed as:

$$\begin{aligned} &\frac{\partial A}{\partial t}+\frac{\partial Q}{\partial x}=q_L, \\ &\frac{\partial Q}{\partial t}+\frac{\partial}{\partial x}\left(\frac{Q^2}{A}+gI_1\right)=g[I_2+A(S_o-S_f)], \end{aligned} \tag{1}$$

where t [T] is the time , x [L] is the longitudinal distance, q_L [L^3T^{-1}] is the lateral inflow per unit width, g [LT^{-2}] is the acceleration due to gravity, S_o [LL^{-1}] is the bed slope, I_1 [L^3] is the hydrostatic pressure force integral, I_2 [L^2] is the integral of the pressure force due to the longitudinal width variations and S_f [LL^{-1}] is the friction slope expressed by means of semi-empirical Manning's law[16].

Additionally to the hydrodynamic equations, the model includes solute transport equations of the form:

$$\frac{\partial(A\phi)}{\partial t}+\frac{\partial(Q\phi)}{\partial x}-E\frac{\partial}{\partial x}\left(A\frac{\partial\phi}{\partial x}\right)-AP_R(\phi)-f=0, \tag{2}$$

where ϕ [Φ] is the cross-sectional average of scalar variable transport, E [L^2T^{-1}] is the longitudinal diffusion-dispersion coefficient, f [ΦL^2T^{-1}] is the load term that accounts for external sources (point and non-point sources) in a water volume and P_R [ΦT^{-1}] is the term used to represent the reactivity of the scalar species transported. The system formed by 1 and 2 can be used to predict the evolution in a forward calculation from initial conditions when suitable upstream and downstream boundary conditions are supplied.

The final purpose of this section is to formulate a method able to determine the boundary condition of a water quality model. The reconstruction is achieved by minimizing the misfit between the model result and the observed data at some target point (x_t). Consequently the objective is to find a set of values that minimize an objective function (or simply a functional) that is expressed as:

$$J(p)=\frac{1}{2}\int_0^T\int_0^L\left[\delta(x-x_t)(\phi(p)-\widehat{\phi})^2\right]dxdt, \tag{3}$$

where p is the variable on which the functional depends, $\delta(x-x_t)$ is the Dirac delta function, $\phi(p)$ is the calculated concentration and $\widehat{\phi}$ is the measured concentration[17]. The variable p can include, in general, different elements such as model parameters (diffusion, decay or roughness coefficients), initial conditions, spill discharges or boundary conditions. The present work is concerned with the application of the technique to explore the sensitivity of the functional to the upstream boundary condition.

Gradient-based methods use information about the local gradient of the functional (∇J) to determine the best estimate of the variable p. The new value at the next iteration can be found by means of an iterative method as:

$$p^{m+1}=p^m-\varepsilon^m(\nabla J)^m, \tag{4}$$

where m indicates the level of the iteration, ε is the step length and ∇J is the gradient of J which can be expressed as:

$$\nabla J=\frac{\delta J}{\delta p}, \tag{5}$$

The adjoint method is a general procedure to calculate the gradient of this functional. When solving the adjoint system, the adjoint state variables are obtained, which are the ones in charge of gathering a global measure of the problem perturbation with respect to the state variables. This will be described in the following sections.

The formulation of the method proposed for the reconstruction of boundary conditions in 1D water quality models has been divided into four levels of complexity: 1) convection-diffusion and reaction of a single constituent, 2) simplified heat balance, 3) Streeter-Phelps model involving CBOD and DO with the presence

of other processes such as sediment oxygen demand (SOD), and 4) nitrification model involving the transport equations of five chemical species plus the temperature.

2.1 Adjoint model of the transport equation

Following the methodology given by Marchuk [18], the adjoint formulation of the scalar transport is addressed. The method begins by multiplying the transport equation (2) by a function σ [ML^{-3}] under the condition that it is differentiable in time and space at least once. Then the result is integrated in the time and space:

$$I=\int_0^T\int_0^L \sigma\left[\frac{\partial(A\phi)}{\partial t}+\frac{\partial(Q\phi)}{\partial x}-E\frac{\partial}{\partial x}\left(A\frac{\partial\phi}{\partial x}\right)-AP_R-f\right]dxdt=0, \tag{6}$$

where $[0,L]$ and $[0,T]$ are the spatial and temporal domains respectively. Using the integration by parts over x and t, eq. (6) leads to:

$$\begin{aligned} I=&\int_0^L \sigma A\phi\Big|_0^T dx-\int_0^T\int_0^L A\phi\frac{\partial\sigma}{\partial t}dxdt+\int_0^T \sigma Q\phi\Big|_0^L dt\\ &-\int_0^T\int_0^L \phi Q\frac{\partial\sigma}{\partial x}dxdt-\int_0^T \sigma AE\frac{\partial\phi}{\partial x}\Big|_0^L dt\\ &+\int_0^T A\phi E\frac{\partial\sigma}{\partial x}\Big|_0^L dt-\int_0^T\int_0^L A\phi E\frac{\partial^2\sigma}{\partial x^2}dxdt\\ &-\int_0^T\int_0^L AP_R dxdt-\int_0^T\int_0^L f dxdt=0. \end{aligned} \tag{7}$$

Therefore, the spatial and temporal derivatives are exchanged from the state the adjoint variable σ. It is possible now to rewrite (3) using (7) as:

$$J=J+I. \tag{8}$$

Assuming that our main interest is to estimate the sensitivity of J with respect to the boundary conditions, variations must be taken with respect to ϕ in such a way that:

$$\delta J=\delta J+\delta I, \tag{9}$$

with:

$$\begin{aligned} \delta I=&\int_0^T\int_0^L\left[-A\frac{\partial\sigma}{\partial t}-Q\frac{\partial\sigma}{\partial x}-AE\frac{\partial^2\sigma}{\partial x^2}-A\frac{\partial P_R}{\partial\phi}\right]\delta\phi dxdt\\ &-\int_0^T \sigma AE\frac{\partial\phi}{\partial x}\delta\phi\Big|_0^L dt+\int_0^T AE\frac{\partial\sigma}{\partial x}\delta\phi\Big|_0^L dt\\ &+\int_0^L \sigma A\delta\phi\Big|_0^T dx+\int_0^T \sigma Q\delta\phi\Big|_0^L dt=0, \end{aligned} \tag{10}$$

and:

$$\delta J=\int_0^T\int_0^L\frac{\partial r}{\partial\phi}\delta\phi dxdt, \tag{11}$$

being $r=\frac{1}{2}(\phi-\widehat{\phi})^2$. In order to eliminate some integrals of (10), initial and boundary conditions are assumed originally undisturbed:

$$\begin{aligned} &\delta\phi(x,T)=\delta\phi(x,0)=0,\\ &\delta\phi(L,t)=0. \end{aligned} \tag{12}$$

In addition, making use of restrictions in the adjoint problem, it is possible to eliminate the sensitivities of [13]:

$$\begin{aligned} &\sigma(x,T)=0,\\ &\sigma(L,t)=0. \end{aligned} \tag{13}$$

Finally, applying the definitions (10) and (11), the restrictions (12) and (13) in Eq. (9) and after some rearrangement, the functional variation is written as follows:

$$\begin{aligned} \delta J=&\int_0^T\int_0^L\left[-A\frac{\partial\sigma}{\partial t}-Q\frac{\partial\sigma}{\partial x}-AE\frac{\partial^2\sigma}{\partial x^2}-\frac{\partial r}{\partial\phi}-A\sigma\frac{\partial P_R}{\partial\phi}\right]\delta\phi dxdt\\ &-\int_0^T\left[\sigma Q\delta\phi\right](0,t)dt. \end{aligned} \tag{14}$$

Therefore, the functional variation with respect to the upstream boundary condition can be represented solely as follows:

$$\nabla J(\phi_0^n)=\frac{\delta J}{\delta\phi}\Big|_{(0,t)}=-Q(0,t)\sigma(0,t). \tag{15}$$

as long as the adjoint equation for the transport of solute is defined as:

$$-A\frac{\partial\sigma}{\partial t}-Q\frac{\partial\sigma}{\partial x}-AE\frac{\partial^2\sigma}{\partial x^2}-\frac{\partial r}{\partial\phi}-A\sigma\frac{\partial P_R}{\partial\phi}=0. \tag{16}$$

With this, the adjoint formulation confirms the ability to evaluate the functional δJ without computing $\delta\phi$ [19].

From (15), the sensitivity of J with respect to the boundary condition of the state variable under study can be useful to recover the information of the boundary condition by means of the gradient descent method by minimizing the error between the calculated and the measured concentration in this case.

It is worth highlighting some additional considerations of eq. (15): first, it is not necessary to perform the integration in space since the information for $\delta\phi(0,t)$ is obtained from a single point (boundary condition). The sensitivity of J with respect to the boundary can be extracted directly from the adjoint solution vector of the corresponding time at $x=0$. On the other hand, the adjoint equation (16) has a structure similar to equation (2), except for a few details. The time-space propagation is different, that is, in the adjoint scheme, the information is conveyed from the final time to the initial time, contrary to the physical scheme. Furthermore, the error r made in the physical problem becomes a source term at x_t in the adjoint problem. Additionally, the form of the decay term changes when moving from the physical problem to the adjoint problem.

2.2 Adjoint model for the heat balance

The transport of the water temperature [°C] (denoted by ϕ_1 in this work) in channels or rivers can be modeled using eq. (2). However, when analyzing the effects of a continuous pollutant load, the effect of dispersion may be ignored since its contribution to the resulting in-stream pollutant concentration is usually small in comparison to the contribution from advection and reaction terms. Therefore, the dispersion term is not included in what follows. In this case the process term P_{R1} represents the heat source term that can be formulated through the relationship ([20–22]):

$$P_{R1} = \frac{H_f}{\rho C_p h}, \tag{17}$$

being ρ [ML^{-3}] is water density, C_p [$L^2T^{-2}\,°C^{-1}$] is heat capacity of water and H_f [MT^{-2}] the net rate of heat exchange expressed as:

$$H_f = K_h(T_e - \phi_1), \qquad T_e = T_d + \frac{R_s}{K_h}, \tag{18}$$

with T_e [°C] the equilibrium river temperature, R_s [MT^{-2}] the solar radiation and K_h [MT^{-2}] the overall water surface heat exchange coefficient. The latter parameter can be expressed by means of the empirical formula given in Table 1 [23].

Table 1 Empirical formulae for computing K_h with: T_a [°C]=air temperature, r_h =relative humidity.

Parameter or coefficient	Expression
Heat exchange coefficient, K_h	$K_h = 4.5 + 0.05\phi + \beta f(U_w) + 0.47 f(U_w)$
Wind function, $f(U_w)$ [LT^{-1}]	$f(U_w) = 9.2 + 0.46U_w^2$
Coefficient β	$\beta = 0.35 + 0.015T_v + 0.0012T_v^2$
Average air temperature, T_v [°C]	$T_v = (\phi_1 + T_d)/2$
Dew point temperature, T_d [°C]	$T_d = 237.3[T_a^* + ln(r_h)]/[17.27 - ln(r_h) - T_a^*]$
	$T_a^* = 17.27T_a/(237.3 + T_a)$

The adjoint problem can also be formulated for this case following the procedure described in Section 2.1. The resulting adjoint equation is similar to eq. (16) with E=0 and $\frac{\partial P_{R1}}{\partial \phi_1}$ defined as:

$$\begin{aligned}
&\frac{\partial P_{R1}}{\partial \phi_1} = \frac{\partial K_h}{\partial \phi}(T_e - \phi_1) + K_h\left(\frac{\partial T_e}{\partial \phi_1} - 1\right),\\
&\frac{\partial K_h}{\partial \phi_1} = 0.05 + f(u_w)\left[\frac{0.0151}{2}(\phi_1 + T_d)\right],\\
&\frac{\partial T_e}{\partial \phi_1} = -\frac{R_s}{K_h}\frac{\partial K_h}{\partial \phi_1}.
\end{aligned} \tag{19}$$

Now, the functional similar to eq. (3) is widespread for K solutes in a general expression:

$$J = \vartheta \int_0^T \int_0^L \sum_{k=1}^{K} r_k, \tag{20}$$

where r_k can be normalized. If it normalizes $r_k = \frac{1}{2}\frac{\left(\phi_k - \widehat{\phi}_k\right)^2}{\left(\widehat{\phi}_{k,(MAX)}\right)^2}$ being $\widehat{\phi}_{k,(MAX)}$ the maximum value of the measurement [24]. It is worth pointing out, that in equation 20 there is the possibility of weighing each chemical species using the parameter ϑ. This is due each chemical species contributes differently to the value of the functional. The weights used when there are several chemical substances are established according to the existing literature. [9,25] The gradient has an expression similar to (15), defined as:

$$\nabla J(\phi_{0,1}^n) = \left.\frac{\delta J}{\delta \phi_1}\right|_{(0,t)} = -Q(0,t)\sigma_1(0,t), \tag{21}$$

which represents the sensitivity of the functional to the temperature of the water at the upstream boundary.

2.3 Modified Streeter-Phelps adjoint model

Water quality is closely related to the deficit of DO [26]. That is the reason why all water quality models consider the evolution of this variable and all the processes in which it is involved. One of the most extended, the modified Streeter-Phelps model, relates the main mechanisms for the DO in a river [27]. For reasons of clarity, the expressions of the proposed model are presented in Appendix I. The terms P_{R2} and P_{R6} of the equations (33) and (34) (from Appendix I) are defined as:

$$\begin{aligned}
P_{R2} &= -R_3 - R_4,\\
P_{R6} &= R_2 - R_3 - R_5,
\end{aligned} \tag{22}$$

being:

$$\begin{aligned}
&\text{Re-aeration}\,(R_2) = k_a\theta_a^{T20}\,(\phi_{sat} - \phi_6)\,,\\
&\text{C-oxidation}\,(R_3) = -k_d\theta_{2d}^{T20}\left(\frac{\phi_6}{k_{BOD} + \phi_6}\right)\phi_2,\\
&\text{C-settling}\,(R_4) = -\frac{v_{s3}\,(1 - f_{d2})}{h}\phi_2,\\
&\text{Sediment } O_2\text{-demand}\,(R_5) = -\frac{SOD}{h}\theta_S^{T20},
\end{aligned} \tag{23}$$

Since the procedure is similar to subsection 2.1 and 2.2, the reader is referred to Appendix I for all the details of the resulting adjoints equations. The adjoint equations using the short notation (36) (from Appendix I) can be described as:

$$C_{A,2} + (\sigma_2 + \sigma_6)A\frac{\partial R_3}{\partial \phi_2} + \sigma_2 A\frac{\partial R_4}{\partial \phi_2} + \frac{\partial r}{\partial \phi_2} = 0, \tag{24}$$

$$C_{A,6} + \sigma_6 A\frac{\partial R_2}{\partial \phi_6} + (\sigma_2 + \sigma_6)A\frac{\partial R_3}{\partial \phi_6} + \frac{\partial r}{\partial \phi_6} = 0, \tag{25}$$

with:

$$
\begin{aligned}
\frac{\partial R_2}{\partial \phi_6} &= -k_a \theta_a^{T20}, \\
\frac{\partial R_3}{\partial \phi_2} &= -k_d \theta_{2d}^{T20} \left(\frac{\phi_6}{k_{BOD} + \phi_6} \right), \\
\frac{\partial R_3}{\partial \phi_6} &= k_d \theta_{2d}^{T20} \frac{k_{BOD}}{(k_{BOD} + \phi_6)^2} \phi_2, \\
\frac{\partial R_4}{\partial \phi_2} &= -\frac{V_{s3}\,(1 - f_{d5})}{h},
\end{aligned}
\tag{26}
$$

and the gradient of both CBOD [ML^{-3}] and DO [ML^{-3}] is:

$$
\nabla J(\phi_{0,k}^n) = \frac{\delta J_k}{\phi_k(0,t)} = -\sigma_k(0,t) Q(0,t). \tag{27}
$$

In this new system, a meaningful aspect is that the adjoint kinetic model given by eq. (24) and (25) is a function of both the adjoint variables and the physical variables, which adds an additional complexity to the adjoint system with respect to the physical system.

2.4 Adjoint model of nitrification

The formulation of the adjoint problem can be extended to a vital process in the control of water quality: the nitrogen cycle. The set of equations can be expressed as[28–30]:

$$
\begin{aligned}
\frac{\partial (A\phi_2)}{\partial t} + \frac{\partial (Q\phi_2)}{\partial x} &= A P_{R2}, \\
\frac{\partial (A\phi_3)}{\partial t} + \frac{\partial (Q\phi_3)}{\partial x} &= A P_{R3}, \\
\frac{\partial (A\phi_4)}{\partial t} + \frac{\partial (Q\phi_4)}{\partial x} &= A P_{R4}, \\
\frac{\partial (A\phi_5)}{\partial t} + \frac{\partial (Q\phi_5)}{\partial x} &= A P_{R5}, \\
\frac{\partial (A\phi_6)}{\partial t} + \frac{\partial (Q\phi_6)}{\partial x} &= A P_{R6},
\end{aligned}
\tag{28}
$$

where ϕ_3, ϕ_4, ϕ_5 [ML^{-3}] are the sate variables water. Organic Nitrogen (ON), Ammonia Nitrogen ($NH_3 - N$) and Nitrate Nitrogen ($NO_3{}^-$) respectively. The decay processes are slightly altered with respect to the simplified Streeter-Phelps model:

$$
\begin{aligned}
P_{R2} &= -R_3 - R_4 - R_9, \\
P_{R3} &= -R_6 - R_7, \\
P_{R4} &= R_6 - R_8, \\
P_{R5} &= R_8 - R_9, \\
P_{R6} &= R_2 - R_3 - \frac{5}{4}\frac{32}{14} R_5 - \frac{64}{14} R_9,
\end{aligned}
\tag{29}
$$

where the numerical coefficients are the consequence of using grams instead of moles to express the concentrations. The processes are defined as:

$$
\begin{aligned}
&\text{ON-mineralization}\,(R_6) = K_{34} \theta_{34}^{T20} \phi_3, \\
&\text{ON-settling}\,(R_7) = \frac{v_{s3}(1 - f_{D3})}{h} \phi_3, \\
&\text{Nitrification}\,(R_8) = K_{45} \theta_{45}^{T20} \phi_4 \left(\frac{\phi_6}{K_{NIT} + \phi_6} \right), \\
&\text{Denitrification}\,(R_9) = K_{5D} \theta_{5D}^{T20} \phi_5 \left(\frac{K_{NO3}}{K_{NO3} + \phi_6} \right),
\end{aligned}
\tag{30}
$$

For the sake of brevity this section is limited to presenting only the adjoint system of each of the variables present in the formulation. The system of adjoint variables using the short notation (36) can be expressed as:

$$
\begin{aligned}
&C_{A,1} - A \frac{\partial P_{R1}}{\partial \phi_1} + \frac{\partial r}{\partial \phi_1} = 0, \\
&C_{A,2} + (\sigma_2 + \sigma_6) A \frac{\partial R_3}{\partial \phi_2} + \sigma_2 A \frac{\partial R_4}{\partial \phi_2} + \frac{\partial r}{\partial \phi_2} = 0, \\
&C_{A,3} + (\sigma_3 - \sigma_4) A \frac{\partial R_6}{\partial \phi_3} + \sigma_3 A \frac{\partial R_7}{\partial \phi_3} + \frac{\partial r}{\partial \phi_3} = 0, \\
&C_{A,4} + (\sigma_4 - \sigma_3) A \frac{\partial R_8}{\partial \phi_4} + \sigma_6 A \frac{64}{12} \frac{\partial R_8}{\partial \phi_4} + \frac{\partial r}{\partial \phi_4} = 0, \\
&C_{A,5} + \left(\sigma_5 + \sigma_2 \frac{5}{4} \frac{32}{14} \right) A \frac{\partial R_9}{\partial \phi_5} + \frac{\partial r}{\partial \phi_5} = 0, \\
&C_{A,6} - \sigma_6 A \frac{\partial R_2}{\partial \phi_6} + (\sigma_6 + \sigma_2) A \frac{\partial R_3}{\partial \phi_6} + \left(\frac{64}{12} \sigma_6 + \sigma_4 - \sigma_5 \right) A \frac{\partial R_8}{\partial \phi_6}, \\
&+ \left(\sigma_5 + \sigma_2 \frac{5}{4} \frac{32}{14} \right) A \frac{\partial R_9}{\partial \phi_6} + \frac{\partial r}{\partial \phi_6} = 0,
\end{aligned}
\tag{31}
$$

where:

$$
\begin{aligned}
\frac{\partial R_6}{\partial \phi_3} &= K_{34} \theta_{34}^{T20}, \\
\frac{\partial R_7}{\partial \phi_3} &= \frac{v_{s3}(1 - f_{D3})}{h}, \\
\frac{\partial R_8}{\partial \phi_4} &= K_{45} \theta_{45}^{T20} \left(\frac{\phi_6}{K_{NIT} + \phi_6} \right), \\
\frac{\partial R_8}{\partial \phi_6} &= K_{45} \theta_{45}^{T20} \left(\frac{K_{NIT}}{(K_{NIT} + \phi_6)^2} \right), \\
\frac{\partial R_9}{\partial \phi_5} &= K_{5D} \theta_{5D}^{T20} \left(\frac{K_{NO3}}{K_{NO3} + \phi_6} \right), \\
\frac{\partial R_9}{\partial \phi_6} &= -K_{5D} \theta_{5D}^{T20} \left(\frac{K_{NO3}}{(K_{NO3} + \phi_6)^2} \right),
\end{aligned}
\tag{32}
$$

System (31) and the target function (20), allows the reconstruction of the variable information in time considering the interrelationships of the cycle of the carbon, nitrogen cycle and heat present in an aquatic ecosystem.

3 Numerical resolution

To solve the fate and transport equation of each chemical species in the physical system, it is necessary that the discretization of the advection-dispersion-reaction equation (2) is combined with the discretization of the flow of the shallow water equations (1) to ensure conservative solutions. The non-linear system of partial differential equations (shallow water and transport equations) can be solved by means of the Godunov scheme based on the resolution of the Riemann problems at each interface between the computational cells. The details of how the Roe scheme linearizes the equations at each interface, maintaining both the equilibrium between the source sources and the stability throughout the simulation period are detailed in Murillo and Navas-Montilla [16], Burguete *et al.* [31], Gordillo *et al.* [32], Morales-Hernández *et al.* [33].

With this numerical scheme, it is possible to update the conserved variables (A, Q and ϕ_k, with $k = 1...6$) at all points of the domain and at all times provided that suitable initial and boundary conditions are supplied. The adjoint equations can be solved using the same scheme, keeping in mind the time-space propagation directions and the feeding of the boundary conditions and source terms.

The flowchart of both the main system (forward) and the adjoint system (backward) to recover the information of the boundary is illustrated in Figure 1. The first step in the control logic is to establish a set of boundary values for all state variables. With this first guess, the physical equation is solved. In this forward resolution, the values of both hydraulic and quality variables are recorded at each time and in the whole domain. The process of recording and calculating the hydrodynamic variables is only done once in the optimization (first run forward). Then, as the iterative process progresses, the transport equation is simply computed with the stored hydrodynamic information. The next step is to evaluate the degree of misfit between the simulated values and the observed values. If the error found is greater than a tolerance, the adjoint variables are calculated by a backward simulation, to provide the direction of descent $\nabla J(\phi^n_{0,k})$. Using this and a constant step length ε, the optimization method determines the new set of values that will enter as a boundary condition for the forward problem. The final step is to evaluate the functional again. If the convergence test is completed, the process stops. Otherwise, it goes back to the second stage. This process will be repeated as many times as necessary in order to reach an expected value of J, or even when there is no significant variation of it. The gradient is used as a measure of the sensitivity that leads the optimizer to a minimum. The efficiency of this process is adequate enough especially when dealing with convex problems. The simplest implementation (following in the work) of the descent gradient method found the descent direction ∇J can be followed in Sun and Yuan [17], Nocedal and Wright [34], Rao [35].

4 Evaluation of the adjoint models

To ensure the reliability and robustness of the adjoint technique, some analytical and real cases are considered. They cover both steady and unsteady configurations and the levels of complexity for the water quality detailed in Section 2.

4.1 Case 1. Reconstruction of a pulse of solute

The purpose of this case is to reconstruct the boundary condition of a Gaussian function with the convection-diffusion and reaction processes. This case corresponds to an ideal situation in a flat, frictionless, 2000 m long rectilinear channel with rectangular cross section and $A = 10\,\mathrm{m}^2$. The cross sectional average flow velocity is $u = 1\,\mathrm{m/s}$. To achieve the objective, the temporal evolution of the concentration is previously recorded at $x_t = 1000$ m with a direct simulation. The upstream concentration pulse for this direct simulation is a Gaussian function with a maximum concentration of 10 $\mathrm{g/m^3}$ at $t = 1000$ s. The solute is transported with a diffusion coefficient $E = 5\ \mathrm{m^2/s}$ and with a decay rate of $5\times10^{-4}\ s^{-1}$ throughout the simulation. With a clear target, the optimization process is switched on. This process starts with a first guess $\phi(0,t) = 0\ \mathrm{g/m^3}$ of the upstream boundary condition to be recovered. For all cases the starting $\varepsilon = 0.01$ has been selected, being reduced in case the functional (or error) grows in two successive iterations. Afterwards, through the iterative method, a new set of values is generated, each time closer to the optimum. In this simple case, the goal of the iterative method will be to recover the Gaussian function describe above.

Figure 2 shows the reconstruction of the boundary condition ($x_0 = 0$) and the target ($x_t = 1000$ m) for several iterations, as well as the functional evolution. Observing the reconstruction of the boundary condition (Figure 2a) the method is able to recover the temporal distribution of the Gaussian function in 50 iterations. This same process is presented in Figure 2b. The target progresses as the number of iterations increases, reaching a result similar to that observed at $x = 1000$ m. Both the reconstruction of the boundary conditions and the target are achieved satisfactorily without presenting any oscillations that might destabilize the final solution. Figure 2c presents the evolution of the functional 3 at each iteration, showing a progressive almost linear decrease that allows the objective to be reached quickly in a few iterations. The technique struggles to recover the shape provided by the measured data. There is not a single rule for the required number of control data points to ensure the successful reconstruction. The more complete this is the best results will be achieved. This first test case uses a few hundreds data.

The next case considers the same hydraulic and chemical conditions but with a discontinuous function for the solute. The exact solution is described in Genuchten *et al.* [36]. The solution assumes a pulse of solute injected at $x = 0$ for a period of 1000 s with the advection and diffusion processes described in the previous case. With the target defined at $x_t = 1000$ m, the reconstruction process of both the spatial and temporal distributions begins with a first guess of $\phi(0,t) = 0\ \mathrm{g/m^3}$.

Figure 3a illustrates the reconstruction of the boundary condition at some iterations. They present small oscillations due to the

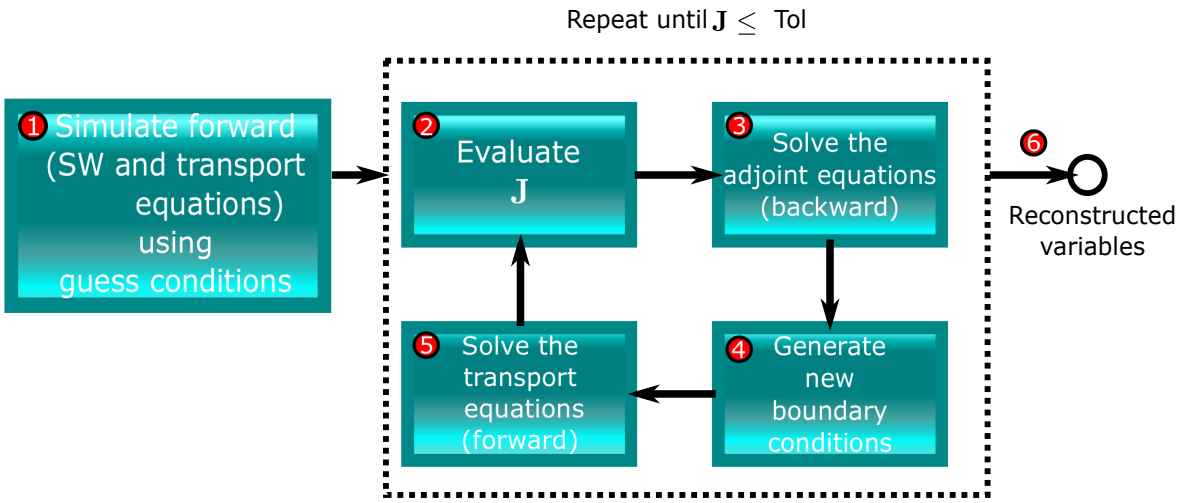

Fig. 1 Flowchart to reconstruct the boundary condition in a water quality model

shape of the original signal. The sharp change in $t = 1000$ s in the function might be the cause of the variations in the last iterations. These differences are completely reduced when the type of function to be reconstructed is smoother as observed in the previous example.

On the other hand, Figure 3b shows the target at $x_t = 1000$ m. The exact solution is successfully captured by the proposed method after 80 iterations. The spatial distribution of the solute concentration at $t = 2000$ s can also be compared against the analytical solution (Figure 3c). As observed, the longitudinal profiles tend to converge to the exact solution progressively and without presenting any instability during the entire optimization process. Regarding the functional (see Figure 3d), the largest decrease is found during the first 20 iterations; after that time the value still diminishes but in a slower way.

4.2 Case 2. Reconstruction of the Streeter-Phelps model variables including the water temperature

This case is proposed to check the adjoint models of Section 2.2 and 2.3 and to observe the effect of point sources on the main channel. The reconstructed numerical distributions can be compared with the original steady state boundary conditions imposed on the problem (described as a reference solution in the different figures shown) and longitudinal output profiles of the QUAL2E model[37] p. 651.

A trapezoidal channel of length 110 km, side slope 2, bottom width 10 m and roughness coefficient of 0.035 is considered. The bottom slope is 2×10^{-4} from 0 m to 50 km and 1.8×10^{-4} onwards. A flow of 5.787 m^3/s, with a temperature of 20 °C, and constant DO and CBOD concentrations of 7.5 and 2 g/m^3, respectively, enter this channel.

The first point source is located at 10 km. A constant discharge flow $Q_{L1} = q_L \Delta x = 0.463$ m^3/s is introduced with a temperature of 28°C, and DO and CBOD concentrations of $\phi_6 = 2.0$ and $\phi_2 = 200$ g/m^3 respectively. The second source is discharged to the main river at $x = 50$ km at a rate of $Q_{L2} = 1.157$ m^3/s, with a temperature of 15°C, and concentrations of DO=9.0 and CBOD=5 g/m^3. The SOD value is 5 $gm^{-2}d^{-1}$ only in the reach between 10 and 30 km. Otherwise, it is set to zero. The processes of both CBOD settling removal rate and de-oxygenation rate are established at 0.25 d^{-1} and 0.5 d^{-1} respectively. The details of the other parameters such as meteorological variables can be found in Chapra[37], p. 651. The target is located at $x_t = 60$ km. At this monitoring station, the quality variables are recorded by solving the equations (2), (33) and (34) simultaneously with the system (1) through a direct simulation. These distributions will be the result of the decay processes of each substance as a function of temperature and external contributions from both point sources as well as weather conditions. The initial conditions of T, CBOD and DO were of 0.0 g/m^3 for this case.

The results after the optimization process are presented in Figures 4 and 5. An early convergence is observed for the reconstruction of the boundary condition of water temperature (Figure 4a). The first 5 iterations are plotted in the graphs in order to show the initial tendency. Around 10 iterations are enough in this case to reduce the error below the prescribed tolerance at the target location. Additional iterations are required to reconstruct the upstream boundary condition used in the forward simulation. The upstream boundary reconstruction of the CBOD (Figure 4c) shows a sudden increase during the first day in the first iterations. This may be due to the external contributions mainly from the first source. A few of them are displayed. As the iterative process progresses, the upstream condition tends to the required constant value. The final reconstruction successfully fits the theoretical concentration after 150 iterations. The reconstruction of the upstream boundary condition of the DO (Figure 4e) shows that the proposed method is able to achieve the constant value of 7.5 g/m^3 in a more uniform way.

Figure 4b shows a variable (in time) water temperature at the target location due to the combined effect of the initial condition assumed ($\phi_1(x,0)$=0°C), the meteorological variables and the sources. These conditions generate an important temperature increase in approximately two days, reaching a steady state from there on. Although the measured target varies over time,

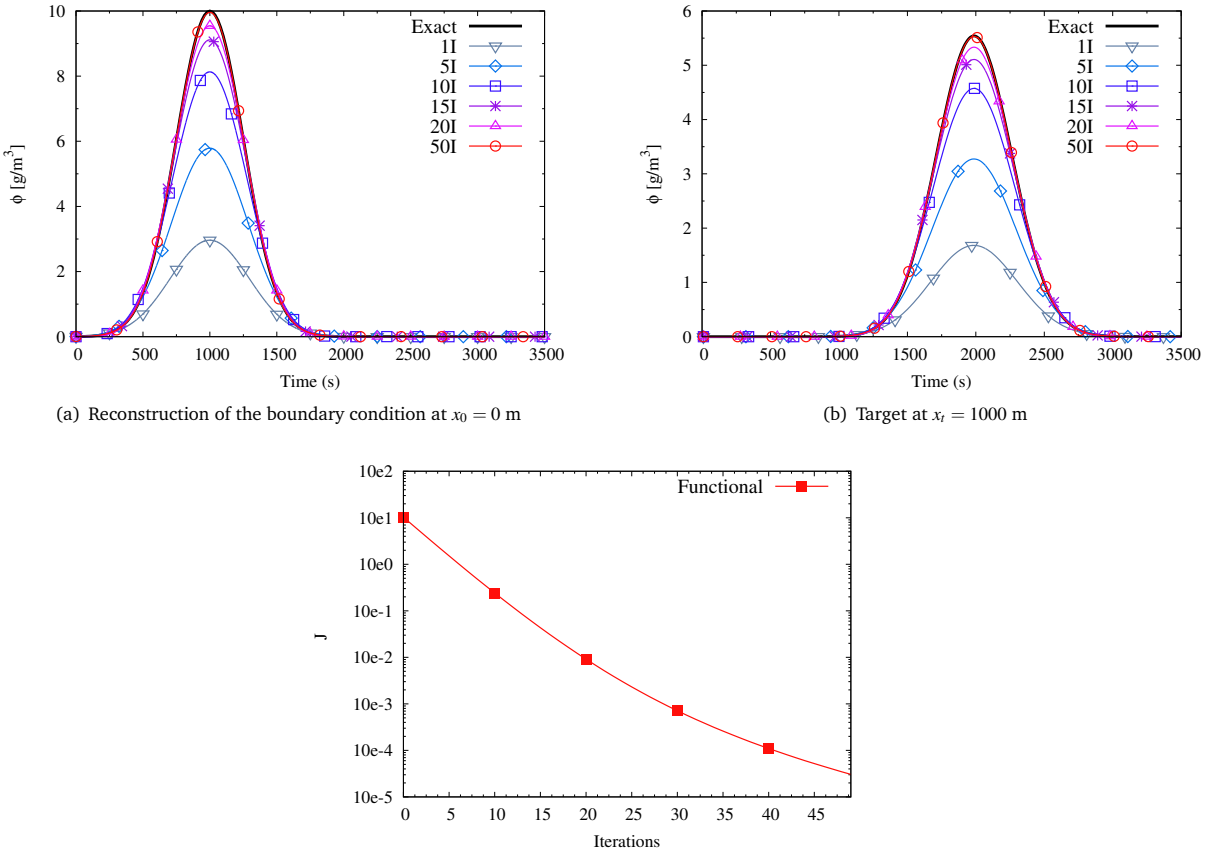

(a) Reconstruction of the boundary condition at $x_0 = 0$ m

(b) Target at $x_t = 1000$ m

(c) Functional evolution

Fig. 2 Case 1. Evolution of reconstructed signals with the analytical solution (Gaussian function) at iterations 1, 5, 10, 15, 20, and 50 and functional evolution.

the method provides an acceptable reconstruction in just 10 iterations. The first 5 iterations are plotted in order to show this tendency. Therefore, even in the presence of lateral inflows with different input values, the proposed objective is achieved. Figure 4d shows the temporal evolution of the target of the CBOD variable at different iterations. The variations during the first two days are attributed to the lateral inflows. This time-varying distribution is fully captured with a good approximation by the technique developed. Additionally the objective of the DO is displayed in Figure 4f. The temporal distribution changes considerably during the first two days. After this time, it becomes steady. This variability is also reconstructed by the method in 150 iterations. In real cases, the upstream boundary condition would not be available for comparison as it is in the test case.

The longitudinal profile of the water temperature reconstructed by the model can be compared with the output distribution of the QUAL2E model (see Figure 5a). The solution at the last iteration clearly demonstrates that both sources and meteorological inputs are correctly formulated in the adjoint scheme. On the other hand, the CBOD distribution (Figure 5b) changes instantaneously at $x = 10$ km, due to the first lateral inflow. This concentration decreases progressively by oxidation of CBOD, displaying a small downward jump at 50 km as a consequence of the second release containing a lower concentration of CBOD than the ambient water. The continuous variability is completely captured as the optimization process progresses. The numerical solution is acceptably close to the value estimated by the QUAL2E model. Figure 5c illustrates the sequence of reconstruction of the DO for some iterations. Note that 150 iterations are required to achieve the reference QUAL2E solution. Figure 5d shows the functional without normalizing. A value of 4.07×10^{-1} is achieved in 150 iterations. In this case, even though the value of the error is not very low, it does not show significant variation in successive iterations. Figure 6 shows the normalized functional. In this case it is observed that the method requires a greater number of iterations to achieve similar results. The cause is due to the amount of error that enters each time step. This value is smaller compared to the error without normalizing. This make it to slow down the optimization. Therefore, using this method it is observed that it is not necessary to adjust the error,[10] contemplating in the following cases an error without normalizing.

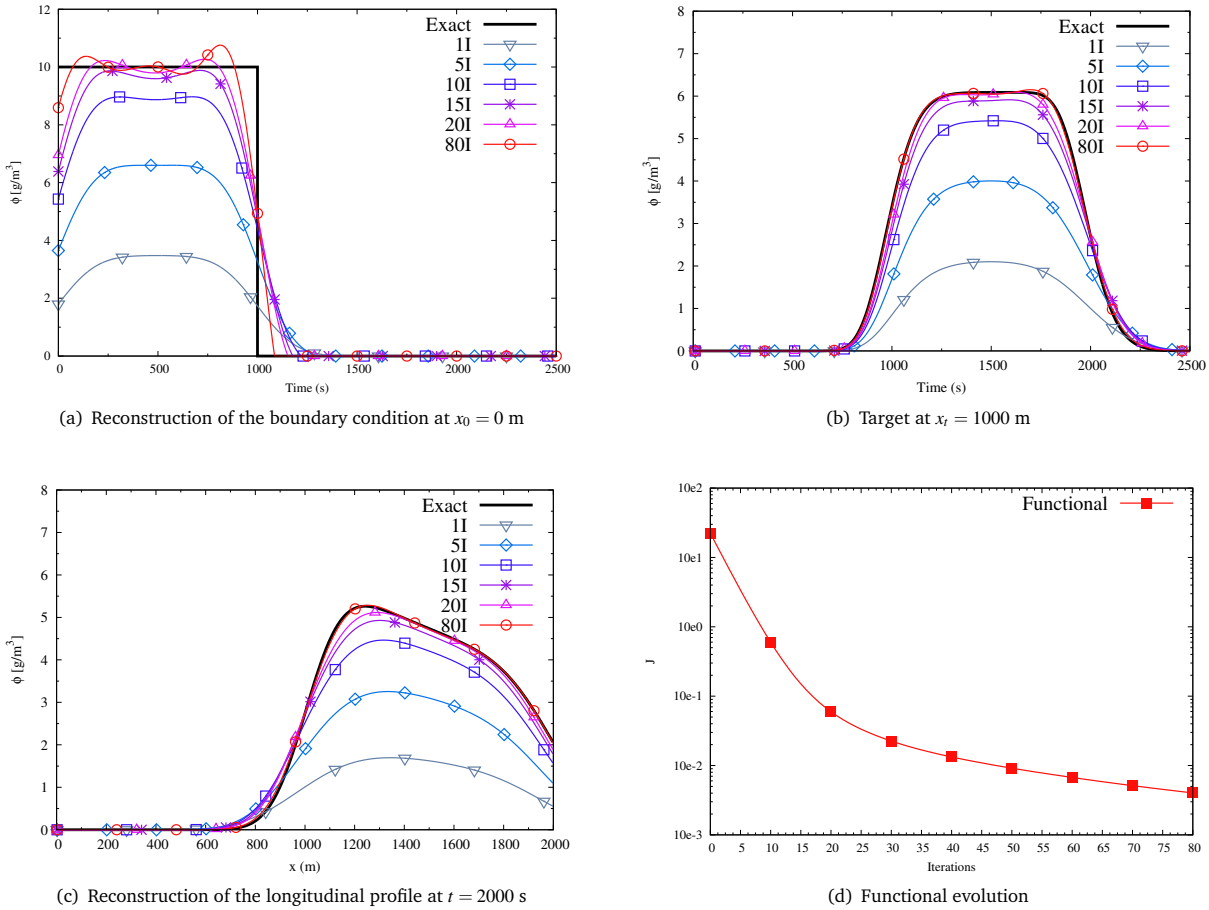

(a) Reconstruction of the boundary condition at $x_0 = 0$ m

(b) Target at $x_t = 1000$ m

(c) Reconstruction of the longitudinal profile at $t = 2000$ s

(d) Functional evolution

Fig. 3 Case 1. Comparison of the numerical solutions with the proposed method with the exact solution at iterations 1, 5, 15, 20 and 50, and functional evolution.

4.3 Case 3. Reconstruction of the Streeter-Phelps model variables with the nitrogen cycle

The example proposed by Thomann and Mueller[30] will be used to illustrate the performance of the technique for the nitrification model. This problem considers a channel of rectangular section of L=50 km, h=1 m y B=30.5 m, with a constant river slope of $S_o = 10^{-4}$ and a Manning coefficient of 0.1 $\mathrm{sm}^{-1/3}$. The flow rate is Q=2.832 m^3/s, with a constant temperature of 25°C, CBOD (ϕ_2)=2 $\mathrm{g/m}^3$, DO (ϕ_6)=8.3 $\mathrm{g/m}^3$, NH_3-N (ϕ_4)=0.2$\mathrm{g/m}^3$, and NO_3 (ϕ_5)=0.5 $\mathrm{g/m}^3$.

The decay coefficients of CBOD and nitrification used for this case are of 0.3 d^{-1} and 0.15 d^{-1} respectively. The only discharge present in this case comes from a treatment plant located at x=1720 m. This source has the following characteristics Q_L=0.328 m^3/s, CBOD (ϕ_2)=80 $\mathrm{g/m}^3$, DO (ϕ_6)=8.3 $\mathrm{g/m}^3$, NH_3-N (ϕ_4)=15 $\mathrm{g/m}^3$, and NO_3 (ϕ_5)=0.5 $\mathrm{g/m}^3$. In order to compare the computed values of total CBOD with the field data of $CBOD_5$, a constant ratio of $CBOD/CBOD_5 = 2$ is considered.

With these conditions, the simulation is run forward recording the targets of the quality variables at x_t = 9.5 km. Once the objectives are defined, the process sketched in Figure 1 is followed. Figure 7 shows both the reference solution and optimized concentrations at the upstream boundary (left) and target node (right) for the DO, $CBOD_5$ and NH_3-N.

The reconstruction of the upstream boundary condition follows the same pattern: there are small variations in the first instants of time, which are totally reduced as the iterative method converges. On the other hand, observing the temporal distributions at $x_t = 9.5$ km, the method captures in an appropriate way all the temporary variations registered at the monitoring station.

Figure 8 shows the comparisons between the compute and the reference solution longitudinal profiles. The three spatial distributions of DO, $CBOD_5$ and NH_3-N are reconstructed, demonstrating that the proposed adjoint formulation is a valid and an accurate tool.

4.4 Case 4. Ebro River

The last case study is focused on a reach of the Ebro River basin (Spain). The reach considered for this study is located between the cities of Alagón and Zaragoza (see Figure 9) along approximately 40 km.

The objective of this transient case is to recover the information of the water temperature T (ϕ_1), DO concentration (ϕ_6) and

NH_3-N concentration (ϕ_4) at the upstream boundary $x_0 = 0$ (point 1 in Figure 9). This reconstruction will be achieved through the measurement registered at $x_t = 40$ km located in Zaragoza (point 2 in Figure 9). This reconstructed information (boundary condition) of the three chemical variables is compared with the sporadic measures available in the period studied at the gauging station of Alagón.

The period included in this scenario ranges from 02/15/2013 to 02/25/2013. The record of the measurements of both the hydrodynamic (h, Q) and chemical variables (T, DO, NH_3-N) was performed with a periodicity of 15 minutes as long as the stations were active. The collection of samples was carried out by two public institutions: Confederación Hidrográfica del Ebro (CHE) and Sociedad Aragonesa de Gestión Ambiental (SARGA). The values of water depth, water discharge, water temperature, as well as the concentrations of DO and NH_3-N were taken from CHE while SARGA measured the meteorological variables.

The reach was discretized using $\Delta x = 126$ m. The Manning coefficient used for this scenario was $n = 0.025$ sm$^{-1/3}$. The decay coefficients used are represented in Table 2. These parameters were previously calibrated based on values taken from the literature[38].

Figure 10 depicts the simulated and measured discharge at the station located in Zaragoza. Significant differences are observed around the 4th and the 5th days. One of the factors that might cause this dissimilarity is the irrigation extraction, which is not quantified in the model.

Figure 11 shows the reconstruction of the quality variables (T, DO and NH_3-N) at the upstream boundary (left) and at the target location (right). The reconstruction of the temperature at x_0=0 m (Figure 11a) in the last iterations follows a similar pattern to the measurements by the public agency. Furthermore, the speed of convergence in an unsteady event is remarkable. Only 20 iterations are required to recover the information of the water temperature with an acceptable accuracy. However, more iterations are necessary to reconstruct the DO and NH_3-N concentrations.

As shown in Figure 11b, the target at $x = 40$ km is reached as long as the number of iterations increases.

Figure 11c shows the reconstruction of the DO concentration at the upstream boundary ($x_0 = 0$ m). There are significant differences during the first 5 days, attributed mainly to the algae processes, which are not simulated[32,39]. These aquatic plants can be generators or consumers of DO in water bodies. Another source of uncertainty is the quality of the data and the measurement method. However, despite these discrepancies, it is possible to reconstruct the objective measured at the downstream monitoring station (see Figure 11 d).

Finally, Figure 11 e shows the reconstructions of the variable NH_3-N only in the last iteration for the sake of clarity. The very noisy distributions are mostly captured by the proposed method. During the first two days, there is no record of this variable (very common situation) but the reconstructed values give an idea of what was the closest situation. Furthermore, the final distribution of NH_3-N at the target location (see Figure 11 f) becomes very close to the measured distribution.

5 Error analysis

In order to determine the performance of the adjoint model, a quantitative analysis was carried out of the error on both the reconstructed boundary conditions and the targets. The evaluation was based on the Root-Mean-Square Error (RMSE) for all the cases presented (Table 3). In general, this analysis shows that RMSE for all the predicted targets presents good agreement with the measured targets. The best results are achieved in Case 2. However the Case 4 shows greater RMSE due to the large number of parameters that need to be calibrated and due to the limited information used from the other state variables such as the CDBO. In what concerns the reconstructed boundaries, the greatest error observed is found in Case 1 (step function). The reason, as previously mentioned, is attributed to the sharp reconstructed shape. The method tends to be less efficient the sharper the reconstructed signal is. A value of 0.497 is achieved in Case 4 (OD reconstuction) when the RMSE of the target is 0.092. This difference could be due to monitoring stations. It is known that the equipment must be periodically calibrated and standardized in order to obtain good metrics. All these results indicate the correct performance of the proposed adjoint method as the RMSE values are within an acceptable range.

6 Conclusions

The present work is devoted to develop and analyze an adjoint approach to reconstruct the boundary condition for the chemical species and the water temperature in a water quality model for both steady and unsteady configurations. Physically based models and their adjoint formulation have been used to build the method so that the optimization module has been based on the gradient descent method. The formulation of the adjoint problem has been divided into several levels of complexity, including the heat equation with all its external contributions, in order to analyze the performance gradually according to the needs and to the available information. This methodology is able to recover the water quality missing information at some point of the domain, as long as there is a clear downstream measurement used as target. The method also requires that all the rest of the hydrodynamic initial and boundary conditions are available to enable the flow simulation. The technique has been successfully applied to both steady and unsteady scenarios, demonstrating its reliability and robustness. The adjoint method has also proved to be efficient to calculate the gradient of a functional with respect to the reconstructed parameter. This feature makes the technique attractive compared to other optimization methods which could be expensive in terms of computational burden. The efficiency lies in the fact that the method solves an extra non-linear system, on the same calculation mesh, producing the same accuracy in the results. All this leads to obtain acceptable solutions on different configurations with little computational effort compared to the trial and error processes that are usually well-established when calibrating a model. Finally, the method can be useful in the design of new quality control points that represent the whole basin in order to guarantee certain quality standards regulated by the Water Framework Directive (WFD).

Table 2 Calibrated and recommended values for Case 4

Parameter	Units	Calibrated value	Recommended value
Carbonaceous de-oxygenation rate (k_d) at 20 °C	day^{-1}	0.2	0.16-0.21
Half-saturation for carbonaceous (k_{BOD})	gO_2/m^3	0.5	0.5
ON-mineralization rate (k_{71}) at 20 °C	day^{-1}	0.075	0.075
Nitrification rate (k_{12}) at 20 °C	day^{-1}	0.11	0.09-0.13
Half-saturation for nitrification (k_{NIT})	gO_2/m^3	0.5	2.0
Denitrification rate (k_{2d}) at 20 °C	day^{-1}	0.089	0.09
Half-saturation for denitrification (k_{NO3})	gO_2/m^3	0.113	0.1
Oxygen reaeration (θ_R)	-	1.024	1.024
BOD decomposition (θ_{BOD})	-	1.047	1.047
Sediment oxygen demand (θ_{SOD})	-	1.08	1.08
Fraction dissolved CBOD (f_{d5})	-	0.22	0.5
Fraction dissolved organic nitrogen (f_{D7})	-	1.0	1.0

Table 3 Quantitative analysis of the adjoint model

Case	Variable	RSME	
		Boundary Conditions	Target
Case 1 (Gaussian function)	-	0.014	0.053
Case 1 (step function)	-	0.796	0.033
	T	0.076	0.002
Case 2	CDBO	0.015	0.00051
	DO	0.052	0.00085
	CDBO	0.048	0.0099
Case 3	DO	0.131	0.0077
	NH_3-N	0.0109	0.0023
	T	0.232	0.0163
Case 4	DO	0.497	0.092
	NH_3-N	0.038	0.0083

Conflicts of interest

There are no conflicts of interest to declare.

Acknowledgements

This work is part of the PGC2018-094341-B-I00 research project funded by the Ministry of Science and Innovation/FEDER. Additionally, Mario Morales-Hernández was partially supported by the U.S. Air Force Numerical Weather Modeling Program.

Appendix I. Adjoint model of Streeter Phelps

The procedure to derive the adjoint equations of the Streeter-Phelps model begins by defining the transport equations for both organic matter and dissolved oxygen:

$$\frac{\partial(A\phi_2)}{\partial t}+\frac{\partial(Q\phi_2)}{\partial x}=AP_{R2}, \tag{33}$$

$$\frac{\partial(A\phi_6)}{\partial t}+\frac{\partial(Q\phi_6)}{\partial x}=AP_{R6}, \tag{34}$$

where and P_{R2} and P_{R6} are decay processes of each species. The details of the complete set of all decay terms are presented in the Appendix II. Notation. The derivation of the adjoint formulation for the Streeter-Phelps model is achieved following the same procedure described for one solute but multiplying equations (33) and (34) by two adjoint variables σ_2,σ_6 (that relate the CBOD and DO variables), followed by an integration by parts and restrictions in the initial/boundary conditions. In order to evaluate the sensitivity of the Streeter-Phelps model with respect to changes in upstream concentration, variations must be taken on both the CBOD (ϕ_2) and DO (ϕ_6):

$$\begin{aligned}\delta I=\int_0^T\int_0^L\Big\{C_{A,2}+\left[A\frac{\partial R_3}{\partial\phi_2}+A\frac{\partial R_4}{\partial\phi_2}\right]\delta\phi_2+C_{A,6}+\left[A\frac{\partial R_3}{\partial\phi_6}+A\frac{\partial R_2}{\partial\phi_6}+\right]\\ \delta\phi_6\Big\}dxdt-\int_0^T\left[\sigma_2Q\delta\phi_2\right](0,t)dt-\int_0^T\left[\sigma_6Q\delta\phi_6\right](0,t)dt=0,\end{aligned} \tag{35}$$

where for clarity $C_{A,k}$ denotes the advective term of the adjoint variables σ_2 and σ_6 , defined as:

$$C_{A,k}=-\frac{\partial(A\sigma_k)}{\partial t}-\frac{\partial(Q\sigma_k)}{\partial x}, \tag{36}$$

Taking the variations in the objective functional J with respect to ϕ_2 and ϕ_6 and gathering this with eq. (35):

$$\begin{aligned}\delta J=\int_0^T\int_0^L\Big\{\Big[C_{A,2}+(\sigma_2+\sigma_6)A\frac{\partial R_3}{\partial\phi_2}+\sigma_2A\frac{\partial R_4}{\partial\phi_2}+\frac{\partial r}{\partial\phi_2}\Big]\delta\phi_2\\ +\Big[C_{A,6}+(\sigma_2+\sigma_6)A\frac{\partial R_3}{\partial\phi_6}+\sigma_6A\frac{\partial R_2}{\partial\phi_6}+\frac{\partial r}{\partial\phi_6}\Big]\delta\phi_6\Big\}dxdt\\ -\int_0^T\sigma_2Q\delta\phi_2dt-\int_0^T\sigma_6Q\delta\phi_6dt=0,\end{aligned} \tag{37}$$

Appendix II. Notation

k_a [T^{-1}]: Reaeration constant.
θ: Temperature coefficient.
ϕ_{sat} [ML^{-3}]: Saturation concentration of oxygen.
k_d [T^{-1}]: Deoxygenation rate at 20 °C.
$T20$: Defined as the difference between water temperature and reference temperature (20°C).
k_{BOD} [ML^{-3}]: Half-saturation constant for oxygen limitation.
s_{s3} [LT^{-1}]: Settling velocity for CBOD.
f_{d2}: Fraction dissolved of CBOD.
SOD [$ML^{-2}T^{-1}$]: Sediment Oxygen Demand.

K_{34} [T^{-1}]: ON-mineralization at 20 °C.
f_{D3}: Fraction dissolved of ON.
K_{45} [T^{-1}] : Nitrification rate at 20 °C.
K_{NIT} [ML^{-3}]: Half-saturation constant for O_2-limitation of nitrification.
K_{5D} [T^{-1}]: Denitrification rate at 20 °C.
K_{NO3} [ML^{-3}]: Half-saturation for O_2-limitation on denitrification.

References

1 J. L. Martin and S. C. McCutcheon, *Hydrodynamics and transport for water quality modeling*, CRC Press, 1998, pp. 64–65.

2 M. K. Sen and P. L. Stoffa, *Global optimization methods in geophysical inversion*, Cambridge University Press, 2013.

3 R. Zou, W.-S. Lung and J. Wu, *An adaptive neural network embedded genetic algorithm approach for inverse water quality modeling*, *Water Resources Research*, 2007, **43**,.

4 A. Azad, H. Karami, S. Farzin, S.-F. Mousavi and O. Kisi, *Modeling river water quality parameters using modified adaptive neuro fuzzy inference system*, *Water Science and Engineering*, 2019, **12**, 45–54.

5 N. D. Katopodes and M. Piasecki, *Site and size optimization of contaminant sources in surface water systems*, *Journal of Environmental Engineering*, 1996, **122**, 917–923.

6 M. Piasecki and N. D. Katopodes, *Control of contaminant releases in rivers. I: Adjoint sensitivity analysis*, *Journal of Hydraulic Engineering*, 1997, **123**, 486–492.

7 M. Piasecki and N. Katopodes, *Containment of deliberate toxic spills in surface waters*, *WIT Transactions on Ecology and the Environment*, 1994, 486–492.

8 M. Piasecki, *Optimization of In-Stream Dissolved Oxygen Via Control of CBOD Loadings Using the Adjoint Method*, *Proceedings of the International Conference on Estuarine and Coastal Modeling*, 2002, 547–565.

9 M. Piasecki, *Optimal wasteload allocation procedure for achieving dissolved oxygen water quality objectives. I: Sensitivity analysis*, *Journal of Environmental Engineering*, 2004, **130**, 1322–1334.

10 M. Piasecki, *Optimal wasteload allocation procedure for achieving dissolved oxygen water quality objectives. II: Optimal load control*, *Journal of Environmental Engineering*, 2004, **130**, 1335–1344.

11 R. M. Neupauer, *Adjoint sensitivity analysis of contaminant concentrations in water distribution systems*, *Journal of Engineering Mechanics*, 2010, **137**, 31–39.

12 Y. Ding and S. S. Wang, *Identification of Manning's roughness coefficients in channel network using adjoint analysis*, *International Journal of Computational Fluid Dynamics*, 2005, **19**, 3–13.

13 B. F. Sanders and N. D. Katopodes, *Adjoint sensitivity analysis for shallow-water wave control*, *Journal of Engineering Mechanics*, 2000, **126**, 909–919.

14 A. Lacasta, M. Morales-Hernández, P. Brufau and P. García-Navarro, *Application of an adjoint-based optimization procedure for the optimal control of internal boundary conditions in the shallow water equations*, *Journal of Hydraulic Research*, 2018, **56**, 111–123.

15 A. Lacasta and P. García-Navarro, *A GPU accelerated adjoint-based optimizer for inverse modeling of the two-dimensional shallow water equations*, *Computers & Fluids*, 2016, **136**, 371–383.

16 J. Murillo and A. Navas-Montilla, *A comprehensive explanation and exercise of the source terms in hyperbolic systems using Roe type solutions. Application to the 1D-2D shallow water equations*, *Advances in Water Resources*, 2016, **98**, 70–96.

17 W. Sun and Y.-X. Yuan, *Optimization theory and methods: nonlinear programming*, Springer Science & Business Media, 2006, vol. 1.

18 G. I. Marchuk, *Mathematical models in environmental problems*, Elsevier, 2011, vol. 16.

19 N. D. Katopodes, *Free-surface Flow: Environmental Fluid Mechanics*, Butterworth-Heinemann, 2018.

20 D. Brady, W. Graves, J. Geyer, E. E. Institute, J. H. U. D. of Geography and E. Engineering, *Surface Heat Exchange at Power Plant Cooling Lakes: Prepared for Edison Electric Institute Research Project*, Edison Electric Institute, 1969.

21 J. E. Edinger, D. W. Duttweiler and J. C. Geyer, *The response of water temperatures to meteorological conditions*, *Water Resources Research*, 1968, **4**, 1137–1143.

22 W. R. Herb and H. G. Stefan, *Modified equilibrium temperature models for cold-water streams*, *Water Resources Research*, 2011, **47**,.

23 R. R. Gu and Y. Li, *River temperature sensitivity to hydraulic and meteorological parameters*, *Journal of Environmental Management*, 2002, **66**, 43–56.

24 J. Burguete, N. Zapata, P. Garcia-Navarro, M. Maikaka, E. Playan and J. Murillo, *Fertigation in Furrows and Level Furrow Systems. I: Model Description and Numerical Tests*, *Journal of Irrigation and Drainage Engineering-ASCE*, 2009, **135**, 401–412.

25 J. Shen and A. Kuo, *Inverse estimation of parameters for an estuarine eutrophication model*, *Journal of Environmental Engineering*, 1996, **122**, 1031–1040.

26 H. Haider, *A Review of Dissolved Oxygen and Biochemical Oxygen Demand Models for Large Rivers*, *Pakistan Journal of Engineering and Applied Sciences*, 2013, **2013**, 127–142.

27 H. W. Streeter and E. B. Phelps, *A study of the pollution and natural purification of the Ohio River*, Us department of health, education, & welfare technical report, 1958.

28 Z.-G. Ji, *Hydrodynamics and water quality: modeling rivers, lakes, and estuaries*, John Wiley & Sons, 2017.

29 G. Liangliang and L. Daoliang, *A review of hydrological/water-quality models*, *Frontiers of Agricultural Science and Engineering*, 2015, **1**, 267–276.

30 R. V. Thomann and J. A. Mueller, *Principles of surface water quality modeling and control*, Harper & Row, Publishers, 1987.

31 J. Burguete, P. García-Navarro and J. Murillo, *Friction term discretization and limitation to preserve stability and conservation in the 1D shallow-water model: Application to unsteady*

irrigation and river flow, *International Journal for Numerical Methods in Fluids*, 2008, **58**, 403–425.

32 G. Gordillo, M. Morales-Hernández and P. García-Navarro, *Finite volume model for the simulation of 1D unsteady river flow and water quality based on the WASP*, *Journal of Hydroinformatics*, 2019.

33 M. Morales-Hernández, J. Murillo and P. García-Navarro, *Diffusion–dispersion numerical discretization for solute transport in 2D transient shallow flows*, *Environmental Fluid Mechanics*, 2018, 1–18.

34 J. Nocedal and S. J. Wright, *Numerical optimization 2nd*, 2006.

35 S. S. Rao, *Engineering optimization: theory and practice*, John Wiley & Sons, 2009.

36 M. T. Genuchten, F. J. Leij, T. H. Skaggs, N. Toride, S. A. Bradford, E. M. Pontedeiro *et al.*, *Exact analytical solutions for contaminant transport in rivers 1. The equilibrium advection-dispersion equation*, *Journal of Hydrology and Hydromechanics*, 2013, **61**, 146–160.

37 S. C. Chapra, *Surface water-quality modeling*, Waveland press, 2008, pp. 175–183.

38 G. L. Bowie, W. B. Mills, D. B. Porcella, C. L. Campbell, J. R. Pagenkopf, G. L. Rupp, K. M. Johnson, P. Chan, S. A. Gherini, C. E. Chamberlin *et al.*, *Rates, constants, and kinetics formulations in surface water quality modeling*, *EPA*, 1985, **600**, 3–85.

39 J. Huang, H. Yin, S. C. Chapra and Q. Zhou, *Modelling Dissolved Oxygen Depression in an Urban River in China*, *Water*, 2017, **9**, 520.

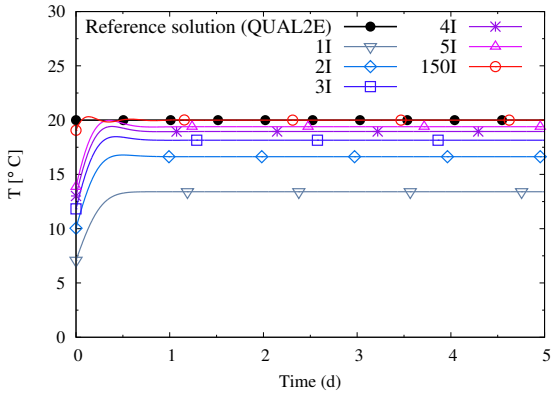

(a) Reconstruction of the boundary condition of T at $x_0 = 0$ m at iterations 1, 2, 3, 4, 5 and 150

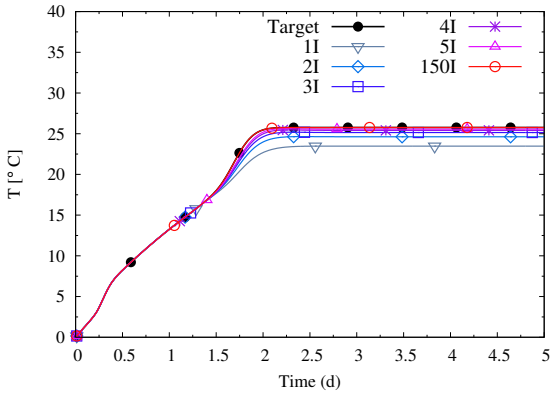

(b) Target of T at $x_t = 60$ km at iterations 1, 2, 3, 4, 5 and 150

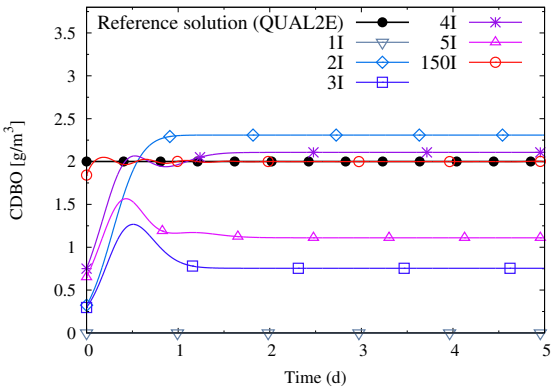

(c) Reconstruction of the boundary condition of CDBO at $x_0 = 0$ m at iterations 1, 2, 3, 4, 5 and 150

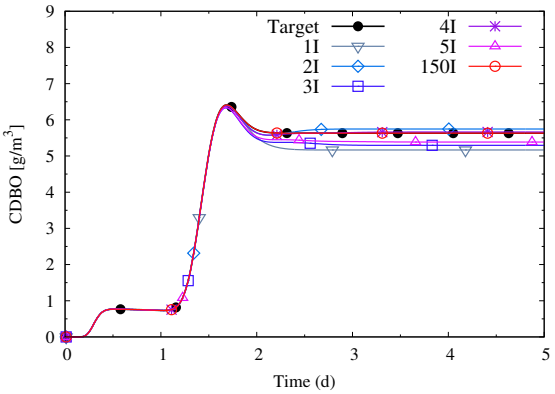

(d) Target of CDBO at $x_t = 60$ km, at iterations 1, 2, 3, 4, 5 and 150

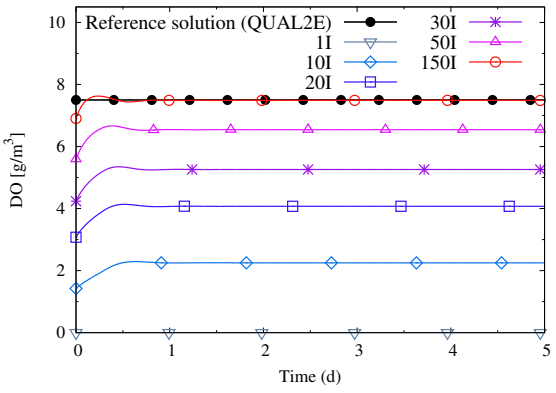

(e) Reconstruction of the boundary condition of DO at $x_0 = 0$ m at iterations 1, 10, 20, 30, 50 and 150

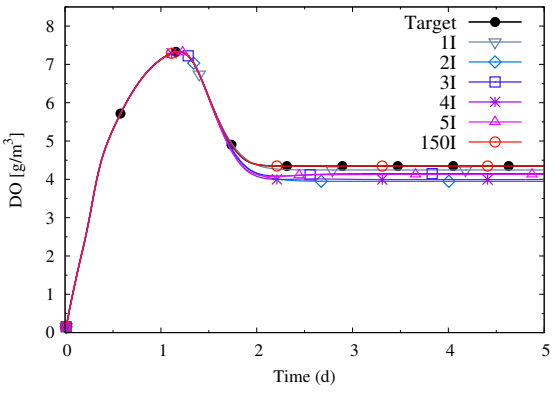

(f) Target of DO at $x_t = 60$ km, at iterations 1, 2, 3, 4, 5 and 150

Fig. 4 Case 2. Comparison of reconstructed boundary conditions (a, c and e) and target (b, d and f) with reference solutions

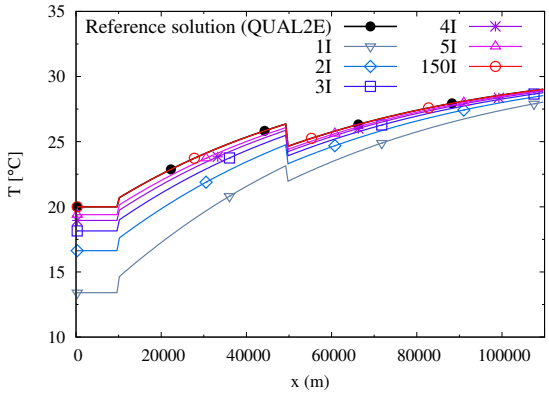

(a) Reconstructed of the longitudinal profile of T at iterations 1, 2, 3, 4, 5 and 150

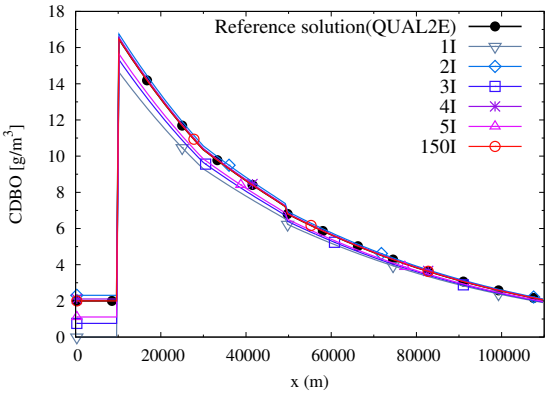

(b) Reconstructed of the longitudinal profile of CBOD at iterations 1, 2, 3, 4, 5 and 150

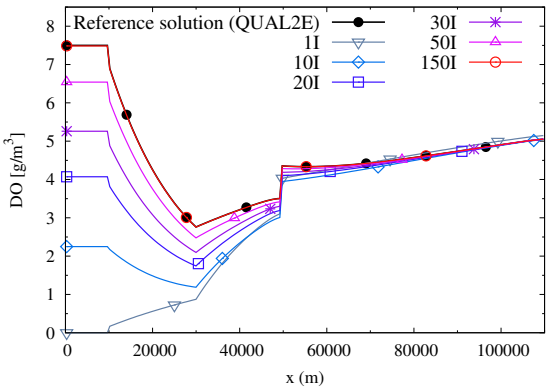

(c) Reconstructed of the longitudinal profile of DO at iterations 1, 10, 20, 30, 50 and 150

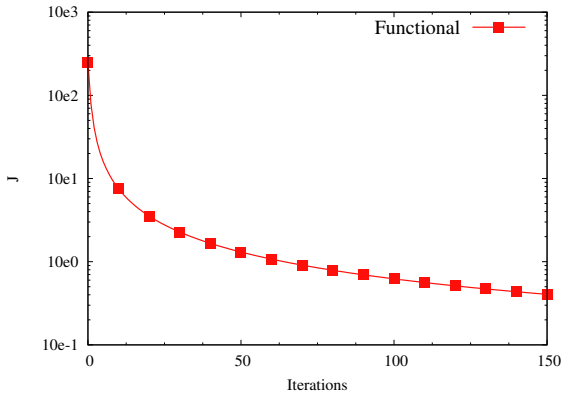

(d) Functional evolution without normalized

Fig. 5 Case 2. Comparison of longitudinal profiles and functional with the output of the QUAL2E model

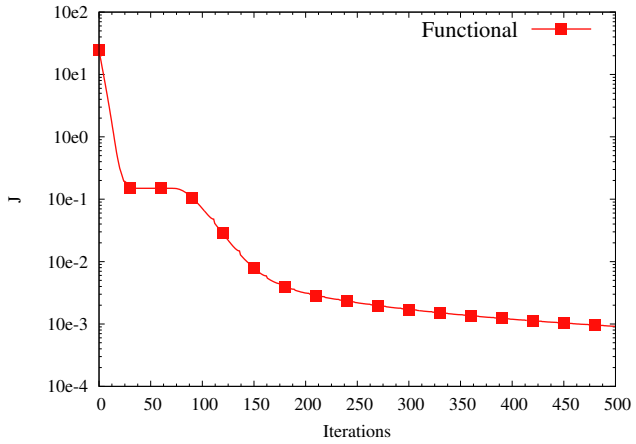

Fig. 6 Case 4. Functional evolution normalized.

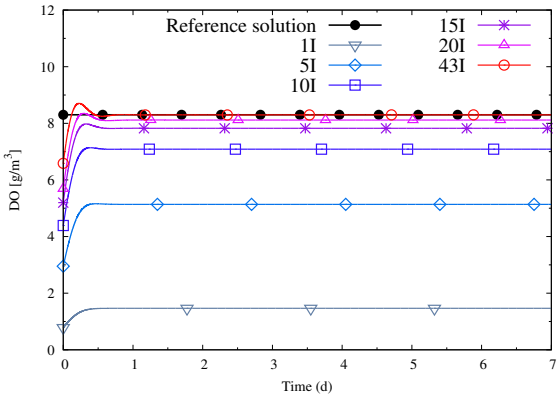

(a) Reconstruction of the boundary condition DO at $x_0 = 0$ m

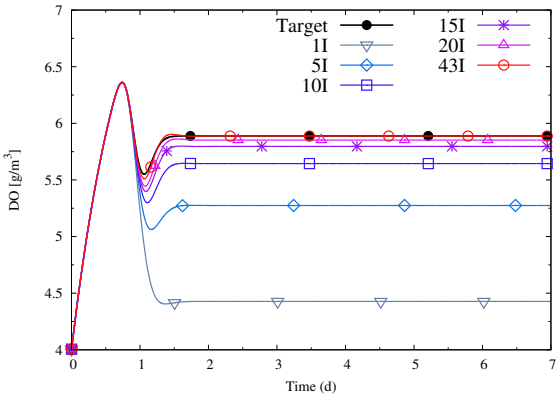

(b) Target of DO at $x_t = 9.5$ km

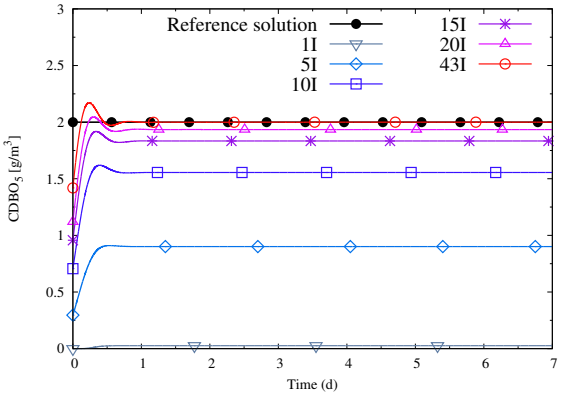

(c) Reconstruction of the boundary condition $CBOD_5$ at $x_0 = 0$ m

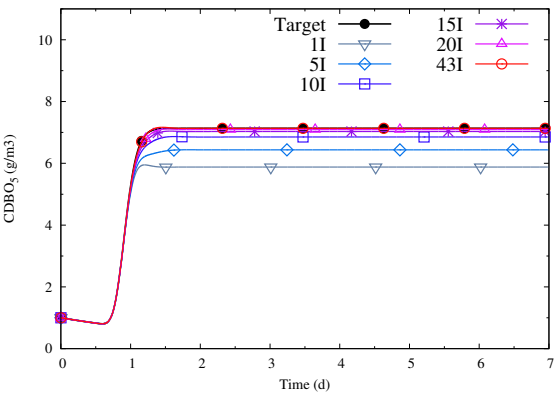

(d) Target of $CBOD_5$ at $x_t = 9.5$ km

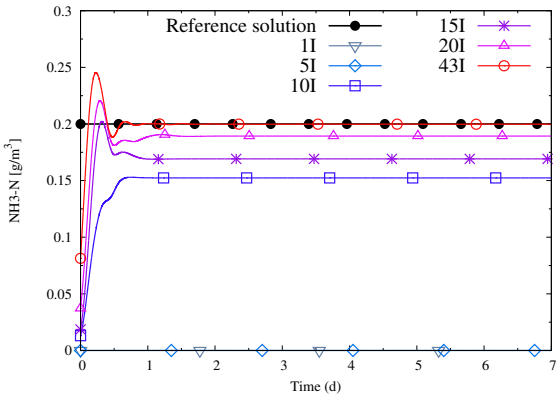

(e) Reconstruction of the boundary condition $NH_3 - N$ at $x_0 = 0$ m

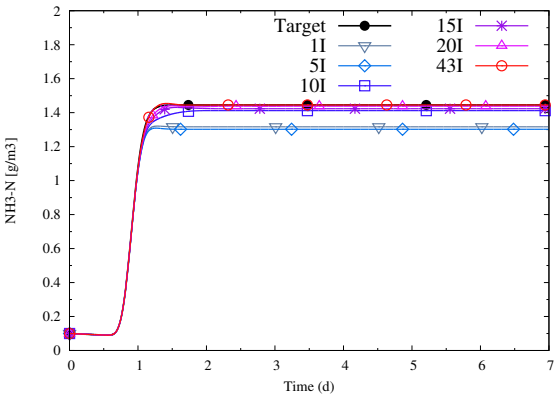

(f) Target of $NH_3 - N$ at $x_t = 9.5$ km

Fig. 7 Case 3. Comparisons of the numerical and reference solutions at both $x_0 = 0$ (a, c and e) and $x_t = 9.5$ km (b, d, and f) at iterations 1, 5, 10, 15, 20 and 43

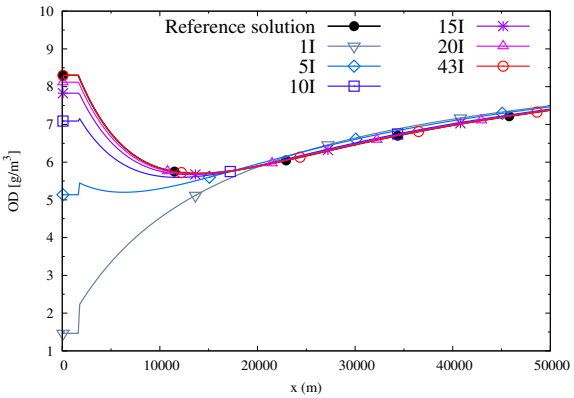

(a) Reconstruction of the longitudinal profile of DO

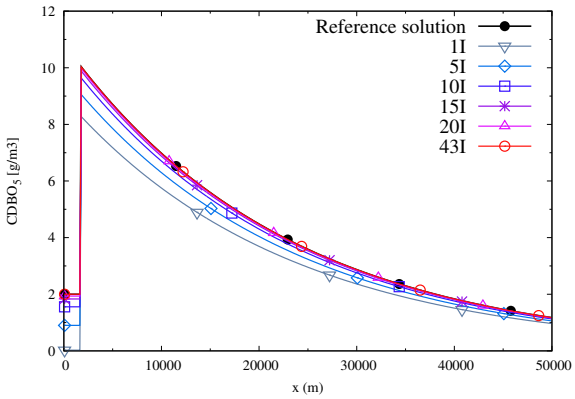

(b) Reconstruction of the longitudinal profile of $CBOD_5$

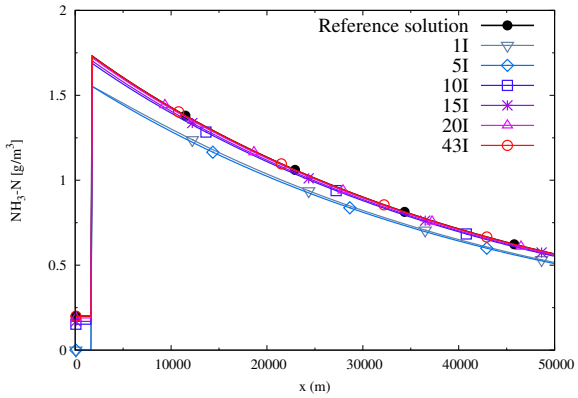

(c) Reconstruction of the longitudinal profile of $NH_3 - N$

Fig. 8 Case 3. Comparison of the longitudinal profiles reconstructed with the observed values at iterations 1, 5, 10, 15, 20 and 43.

Fig. 9 Case 4. Alagón-Zaragoza study reach

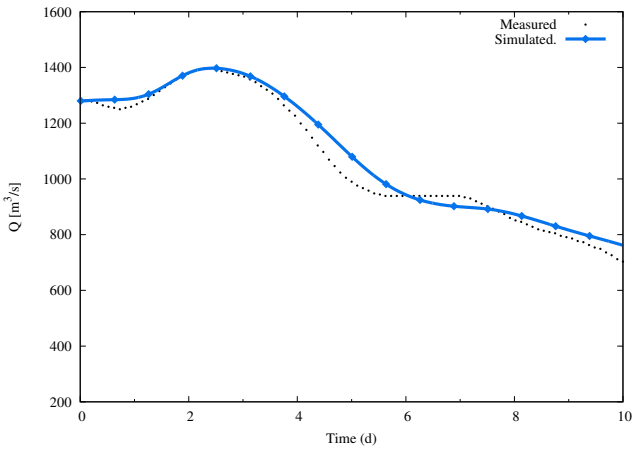

Fig. 10 Case 4. Comparison between measured and simulated flow discharge at Zaragoza gauge station.

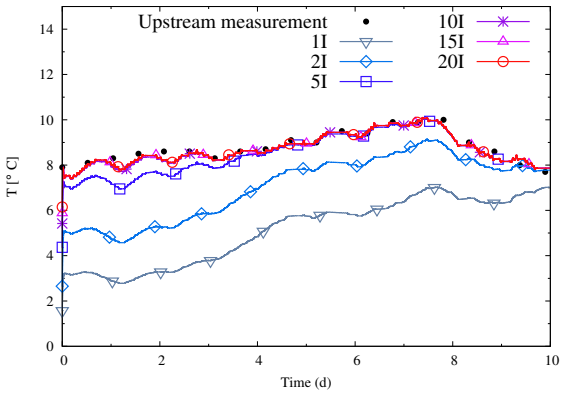

(a) Reconstruction of the boundary condition T at $x_0 = 0$ m at iterations 1, 2, 5, 10, 15 and 20

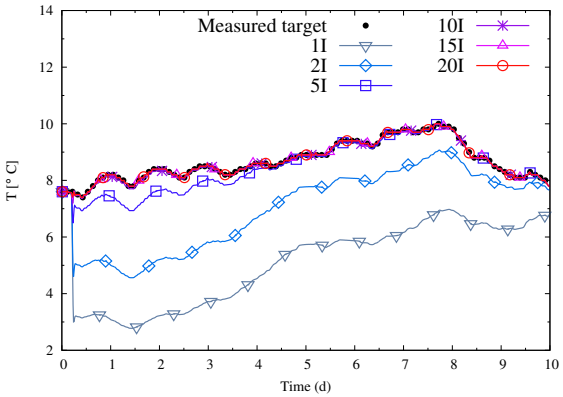

(b) Target of T at $x_t = 40$ km at iterations 1, 2, 5, 10, 15 and 20

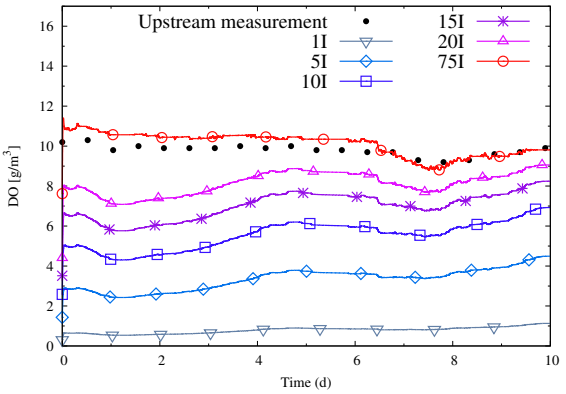

(c) Reconstruction of the boundary condition DO at $x_0 = 0$ m at iterations 1, 5, 10, 15, 20 and 75

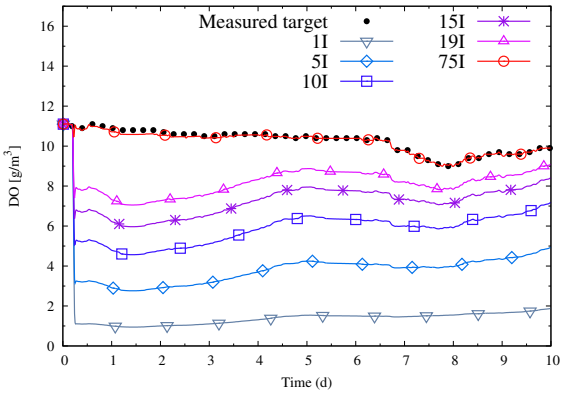

(d) Target of DO at $x_t = 40$ km at iterations 1, 5, 10, 15, 20 and 75

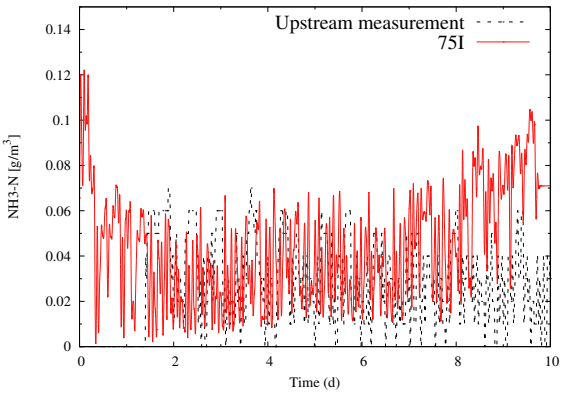

(e) Reconstruction of the boundary condition $NH_3 - N$ at $x_0 = 0$ m at iterations 75

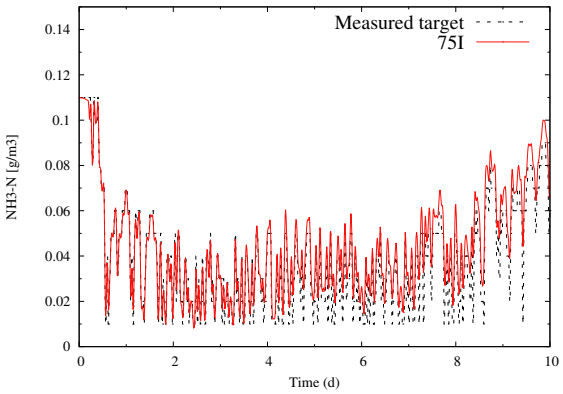

(f) Target of $NH_3 - N$ $x_t = 40$ km at iteration 75

Fig. 11 Case 4. Comparisons of numerical optimized concentration with measurements in both $x_0 = 0$ m (a, c and e) and $x_t = 40$ km (b, d and f).